Electronic Supplementary Material (ESI) for RSC Advances.

This journal is © The Royal Society of Chemistry 2016

Supporting Information

From diffusive to ballistic Stefan-Boltzmann heat transport in thin non-crystalline films

Andreas Makris, Tobias Haeger, Ralf Heiderhoff, Thomas Riedl*

S1 Thin film preparation

In order to perform out-of-plane heat transport analysis we used a step-like film matrix on top of a Silicon substrate with a high thermal conductivity (150 W/(mK) [S1]). With help of ALD (Beneq TFS 200) non-crystalline Al_2O_3 and TiO_2 films were deposited. The thin films were grown from Trimethylaluminium (TMA) and H_2O. Both materials were let into the reaction chamber as gas pulses with a duration of 150 ms followed by a 5 s nitrogen purge after each pulse. The deposition of structured TiO_2 films was carried out in a similar process using Titanium tetrachloride ($TiCl_4$) and H_2O.

In order to create step-structured ALD layers we have firstly masked the substrate with a usual lumocolor pen (Figure S1a). Afterwards the first ALD process took place (Figure S1b) followed by an additional masking step (Figure S1c) and a further ALD process (Figure S1d). These steps can be repeated until the desired structure is prepeared. Afterwards, the areas which were masked with the lumocolor pen, can be lifted off in isopropanol and actenoe and one will get a step structure (Figure S1f). The film thicknesses were determined by use of a Dektak150 surface profiler.

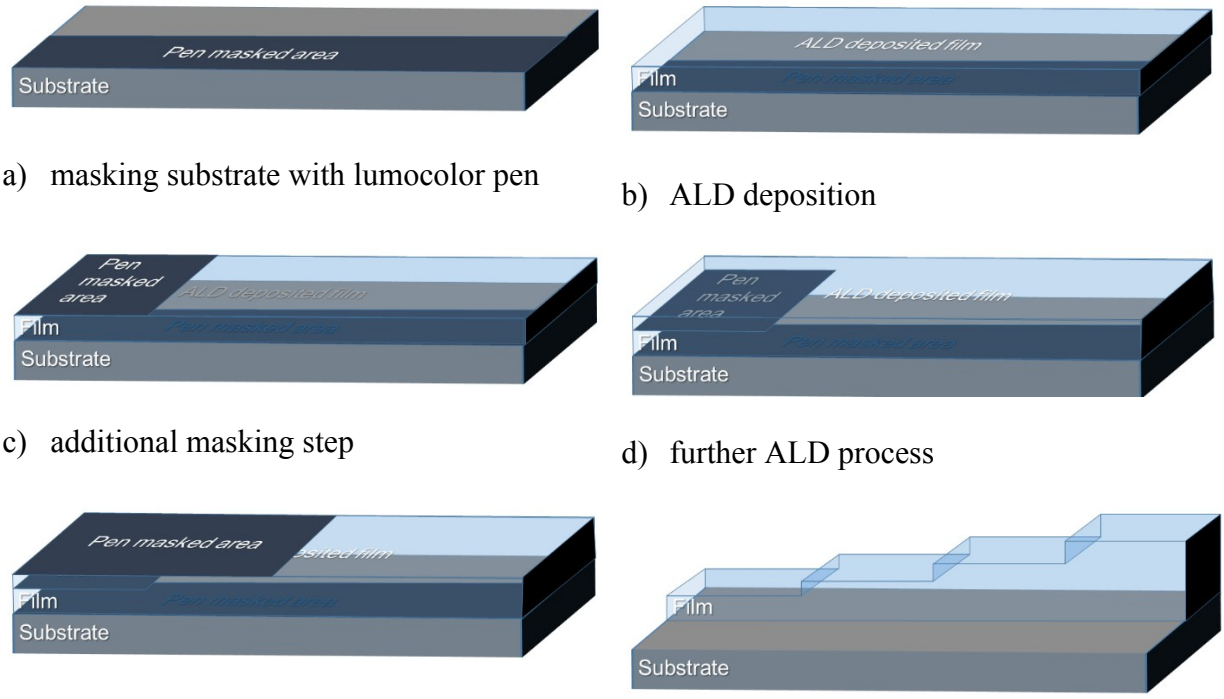

a) masking substrate with lumocolor pen

b) ALD deposition

c) additional masking step

d) further ALD process

e) repeating masking and ALD deposition

f) final layered structure by washing off with Isopropanol and Acetone

Figure S1. *Workflow to create step-like structured ALD layers. The step-like matrix allows to measure a direct difference of thermal properties between films of varied thickness in direct relation to the substrate.*

S2 Scanning near-field thermal microscopy

The SThM used in these thermal conductivity experiments is based on an AFM with laser deflection method (Figure S2). A resistive probe (commercially available VITA-SThM (Bruker) probe) is integrated into this AFM and is connected to a Wheatstone bridge. Calibrating the system the output maximum of the bridge was determined to be $0.29\frac{\mu V}{K}$ with a temperature oscillation amplitude sensitivity of $8\frac{mK}{\sqrt{Hz}}$ limited by the maximal probe current. According to Altes et al. [S2] and Geinzer [S3], the contact can be considered as an aperture under near-field conditions and the bended thermal resistive wire of the probe can be considered as a line-shaped nanoscale heat source (line-shaped nanoscale heat detector) as illustrated in Figure S3. Therefore, the probe generates a heat wave of frequency 2ω with cylindrical

symmetry in a certain frequency range. The lower and upper cut off frequencies were measured to be 3 kHz and 7.2 kHz respectively.

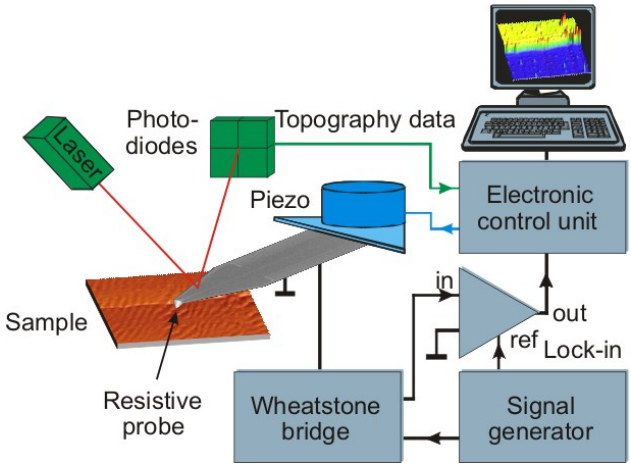

Figure S2. *Schematic of experimental setup.*

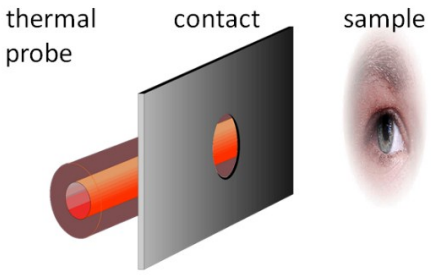

Figure S3. *Detecting the source characteristic under near-field conditions* [S2].

Therefore, the input of the Wheatstone bridge is connected to a signal generator at an applied frequency of 3.3 kHz and the output signal is amplified by a lock-in-amplifier (LIA) for signal to noise ratio (SNR) enhancement and recorded by an electronic control unit (ECU). The frequency selective and phase sensitive detection of the thermal signal is obtained by connecting the signal generator to the reference input of the LIA. The ECU is controlling the XYZ-piezo assembly to guarantee a constant low force between probe and sample [S4].

In order to measure $\Delta\hat{T} = \hat{T}_{film} - \hat{T}_{substrate}$ with a high sensitivity the Wheatstone bridge was balanced when the probe was positioned in contact with the substrate. For further SNR enhancement by averaging and integration, two-dimensional maps of the probe temperature oscillation for different film thicknesses are obtained. Line measurements in vertical direction to the thin film on substrate gradations were integrated and afterwards illustrated in a diagram.

The measured integrated data on the film were averaged for the regions where the probe was on the film and where the probe was on the substrate which could also be detected from the topography image. $\Delta\hat{T}$ was determined afterwards by the difference of these both signals.

S3 Diffusive out-of-plane heat transport

The measured data were compared with calculated and fitted curves in order to describe the heat transport by diffusive out-of-plane heat transport as illustrated in Figure S4.

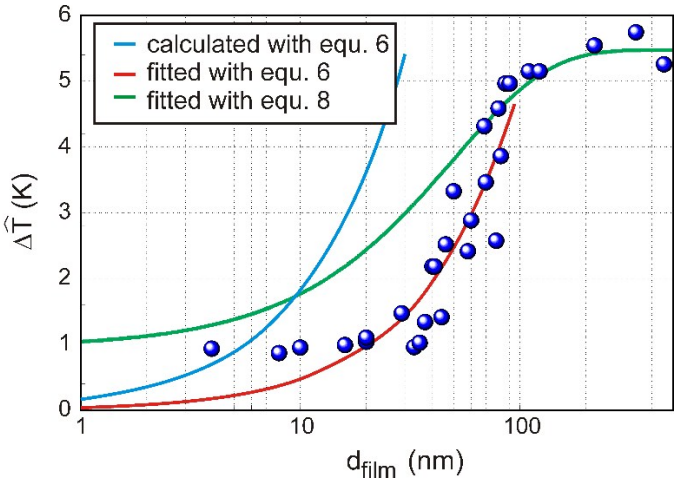

Figure S4. *Comparison of fitted curves using equations 6 and 8. In addition the calculated curve from equation 6 using* $\hat{P} = 4\frac{W}{m}$, $\lambda_{Al_2O_3} = 0.8\,\frac{W}{mK}$, and $w = 100\,nm$ *is illustrated.*

Fitting the measured data according to equation 6 a $\Delta\hat{T} = (0.048 \pm 0.001)\frac{K}{m} \cdot d_{film}$ will be obtained. This will lead to an amplitude of the generated heat power per unit length $\hat{P} = 3.9 \cdot 10^{-9}\frac{W}{m}$ for $\lambda_{Al_2O_3} = 0.8\,\frac{W}{mK}$ and $w = 100\,nm$, which is 9 orders of magnitude less than the calculated value from $\Delta\hat{T}_{max} = \frac{\hat{P}}{\lambda_{film}}$. Alternatively, a significant **increase** of the thermal conductivity up to $8 \cdot 10^{8}\frac{W}{mK}$ or a width of the probe of 25 cm must be considered - both do not make any sense. Note Equations 6 and 7 result from models based on quantitative heat transfer. In addition, the estimate of a decrease of the effective λ_{film} has recently been derived

by a variational approach to solve the BTE. [24] Taking all this together, we do not obtain a better fit to the data as that shown by the empirical model using equation 8. Rather the deviation to the measurement are even higher.

S4 Stefan-Boltzmann like heat transfer

In order to prove Stefan-Boltzmann like heat transfer in analogy to [S5,S6] the SThM probe temperatures were measured at different electrical powers P_{electr} applied to heat the probe. The temperatures were detected at steady state conditions in non-contact in vacuum T_{vac} as well as in contact on a 10 nm thick film T_{film} to take the heat dissipation into the supply lines of the thermal probe into account. At moderate temperatures the radiation heat transfer between our probe and chamber walls is negligible as only under extreme near-field conditions a significant radiative heat transport occurs. The amount of blackbody radiative transfer of thermal energy (a conductance of 250pW/K according to Ref. [21]) is 4 orders less at gaps of 10 nm than diffusive heat transport (calculated to be 1.04 μW/K respectively) on films with a thickness of 10 nm. In addition, the thermal capacity of C_{suppl} is temperature independent and is given by $C_{suppl} = \frac{dQ_{suppl}}{dT}$, where dQ_{suppl} is the change of the stored heat, equation (2) will finally lead in vacuum to

$$C_{suppl} \cdot \frac{dT}{dt} = \dot{Q}_{electr} - \dot{Q}_{suppl} = 0 \quad \text{at steady state condition} \tag{S1}$$

$$\Rightarrow P_{electr} = \lambda_{suppl} \cdot \frac{A_{suppl}}{l_{suppl}} \cdot (T_{vac} - T_0) \tag{S2}$$

where λ_{suppl}, A_{suppl}, and l_{suppl} are the effective thermal conductivity, the cross-sectional area, and the length of the supply lines and T_0 is the room temperature (thermal reservoir). The dependency of the average probe temperature T_{film} at steady state condition in contact with the 10 nm thick film can be found in a similar way to A. A. Wilson et al. [S12] as:

$$\dot{Q}_{electr} = \dot{Q}_{suppl} + \dot{Q}_{sample} \tag{S3}$$

$$\Rightarrow P_{electr} = \frac{1}{R^{th}_{suppl}} \cdot (T_{film} - T_0) + \frac{1}{R^{th}_{contact} + \frac{R^{th}_{diff} \cdot R^{th}_{Stefan-Boltzmann}}{R^{th}_{diff} + R^{th}_{Stefan-Boltzmann}}} \cdot (T_{film} - T_0) \tag{S4}$$

where $\dot{Q}_{sample}$ is the heat flow through the film into the substrate. The first term on the right of S4 represents the diffusive heat transport through the supply lines. $R^{th}_{contact}$ is the thermal contact resistance of the probe on the film. R^{th}_{diff} governs the probability and the amount of diffusive heat transport through the thin film $\dot{Q}_{film} = \left(1 - e^{-\frac{d_{film}}{\Lambda_{film}}}\right)\frac{\lambda_{film} \cdot \pi r^2_{contact}}{d_{film}}(T_{surface} - T_0)$ assuming one-dimensional heat transport across the film. $T_{surface}$ is the surface temperature on the film. λ_{film}, Λ_{film}, and d_{film} are the thermal conductivity, the phonon mean-free path, and the thickness of the film. $r_{contact}$ is the radius of the effective contact area of the probe.

$R^{th}_{Stefan-Boltzmann}$ depends on $T_{surface}$ and determines the contribution of Stefan-Boltzmann like heat transport of phonons [S7] multiplied with its relative weight as

$$\dot{Q}_{Stefan-Boltzmann} = e^{-\frac{d_{film}}{\Lambda_{film}}} \sigma A^{Stefan-Boltzmann}_{contact}\left(T^4_{surface} - T^4_0\right) \tag{S5}$$

where $A^{Stefan-Boltzmann}_{contact}$ is the effective contact area for ballistic heat transport ($\frac{1}{R^{th}_{Stefan-Boltzmann}} = e^{-\frac{d_{film}}{\Lambda_{film}}} A^{Stefan-Boltzmann}_{contact} \cdot \sigma \cdot \left(T^3_{surface} + T_0 T^2_{surface} + T_{surface} T^2_0 + T^3_0\right)$). σ was already calculated by Swartz and Pohl [S8] and is given by:

$$\sigma = \frac{\pi^2 k_B^4}{120\hbar^3} \sum_i \frac{1}{c_i^2} \tag{S6}$$

Here, k_B is Boltzmann's constant, $\hbar$ is the reduced Planck constant, and c_i is the velocity of sound for the respective mode. These phonon velocities can be related to the specific heat [S7] as

$$\sigma = \frac{C \cdot c_i}{16T^3} \tag{S7}$$

As the same electrical power P_{electr} is applied to the SThM probe in contact and non-contact we finally get

$$\begin{aligned}\frac{1}{R_{suppl}^{th}} \cdot (T_{vac} - T_0) = \frac{1}{R_{suppl}^{th}} \cdot (T_{film} - T_0) \\ + \frac{1}{R_{contact}^{th} + \frac{R_{diff}^{th} \cdot R_{Stefan-Boltzmann}^{th}}{R_{diff}^{th} + R_{Stefan-Boltzmann}^{th}}} \cdot (T_{film} - T_0) \\ = \frac{R_{diff}^{th} + R_{Stefan-Boltzmann}^{th}}{R_{diff}^{th} \cdot R_{Stefan-Boltzmann}^{th}} (T_{surface} - T_0)\end{aligned} \tag{S8}$$

It should be noted that in case of a 10 nm thick non-crystalline Al_2O_3 film where $\frac{\sigma}{\lambda_{film}} = 2.4 \cdot 10^{17} \frac{1}{mK^3}$ (using sound velocities $c_{longitudinal}$ of 8700 m/s [S9]) and Λ_{Al2O3}=0.47 nm [S10], at $T_{surface} = 400\ K$, $A_{contact}^{Stefan-Boltzmann} = \pi r_{contact}^2$, the contribution of ballistic transport is 2.4×10^8 time larger than diffusive heat transport (R_{diff}^{th} is parallel to $R_{Stefan-Boltzmann}^{th}$) even when the probability of Stefan-Boltzmann like heat transport is very small as

$$\frac{\dot{Q}_{Stefan-Boltzmann}}{\dot{Q}_{diffusive}} = d_{film} \cdot \frac{e^{-\frac{d_{film}}{\Lambda_{film}}}}{\left(1 - e^{-\frac{d_{film}}{\Lambda_{film}}}\right)} \cdot \frac{\sigma}{\lambda_{film}} \left(T_{surface}^3 + T_0 T_{surface}^2 + T_{surface} T_0^2 + T_0^3\right) \tag{S9}$$

Therefore, S8 can be approximated by

$$\Rightarrow \frac{1}{R_{suppl}^{th}} \cdot (T_{vac} - T_{film}) = \frac{1}{R_{contact}^{th} + \frac{R_{diff}^{th} \cdot R_{Stefan-Boltzmann}^{th}}{R_{diff}^{th}}} \cdot (T_{film} - T_0)$$

$$= \frac{R_{diff}^{th}}{R_{diff}^{th} \cdot R_{Stefan-Boltzmann}^{th}} (T_{surface} - T_0) \quad \text{(S10)}$$

$$\Leftrightarrow \frac{1}{R_{suppl}^{th}} \cdot (T_{vac} - T_{film}) = \frac{1}{R_{contact}^{th} + R_{Stefan-Boltzmann}^{th}} \cdot (T_{film} - T_0)$$

$$= \frac{1}{R_{Stefan-Boltzmann}^{th}} (T_{surface} - T_0) \quad \text{(S11)}$$

Furthermore, it should be noted that no temperature gradient within the film occurs in case of dominant ballistic Stefan-Boltzmann like heat transport [S7]. Therefore, $T_{surface}$ is equal to T_{film} at contact areas responsible for ballistic heat transport as can be depicted from Figure S5. The other areas are negligible as the surface temperature $T_{surface}$ is less than T_{film}. Consequently we get:

$$\frac{1}{R_{suppl}^{th}} \cdot (T_{vac} - T_{film}) = e^{-\frac{d_{film}}{\Lambda_{film}}} \sigma A_{contact}^{Stefan-Boltzmann} (T_{film}^4 - T_0^4) \quad \text{(S12)}$$

.

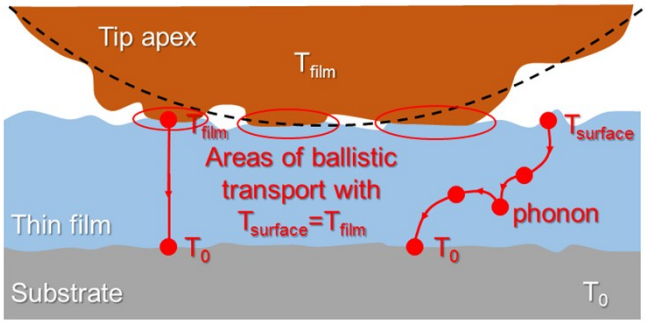

Figure S5. *Illustration of tip apex on thin film. The indicated contact areas are estimated to dominate Stefan-Boltzmann heat transport as* $T_{surface} = T_{film}$. *Ballistic and diffusive heat transport mechanisms of phonons as described by A. Majumdar* [S7] *are visualized in addition.*

The transition of the dominating ballistic regime, which is indicated by a constant $\Delta\hat{T}$ due to a film thickness independent Stefan-Boltzmann like heat transport, to the regime where heat

transport through the thin film will become diffusive is taken to estimate Λ_{film} for non-crystalline Al_2O_3 and TiO_2 films as illustrated in Figure S6.

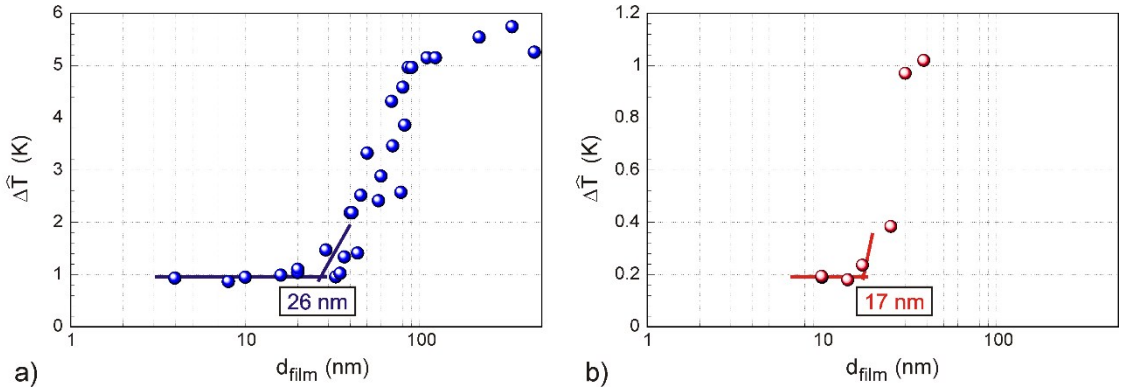

Figure S6. *Determination of film thicknesses (a) d_{film} = 26 nm for Al_2O_3 and b) d_{film} = 17 nm for TiO_2) where heat transport through the thin film will end to be dominated by ballistic Stefan-Boltzmann like mechanisms.*

TiO_2 has higher thermal conductivity than Al_2O_3, as can be directly detected from the saturation value of $\Delta\hat{T}$ for thick films (bulk limit). Using the 3ω-technique we found the thermal conductivity of our non-crystalline TiO_2 bulk material is $\lambda_{TiO_2} = 3.6\frac{W}{mK}$ on a 300 nm ± 6 nm film. This is in agreement for non-crystalline TiO_2 films compared to several other literature data as summarized in [S11].The value of constant $\Delta\hat{T}$ of thin-film and probe for ultra-thin films is one order less for TiO_2, indicating a less surface roughness in this case. The lower surface roughness can also be concluded from diffusion heat transport investigations for a certain range of sample thermal conductivity [S12] as $r_{contact}$ and the thermal contact resistance are constant. The intersections of the constant $\Delta\hat{T}$ of ballistic transport behaviors and the onsets of the increase of $\Delta\hat{T}$ were determined to be $d_{film} = 26\ nm$ for Al_2O_3 and $d_{film} = 17\ nm$ for TiO_2. Finally, Λ_{film} can be estimated assuming $A_{contact}^{Stefan-Boltzmann} \approx \pi r_{contact}^2$ by

$$\left(\lambda_{film} \cdot \frac{\pi r_{contact}^2}{d_{film}}\right) \cdot (T_{film} - T_0) = e^{-\frac{d_{film}}{\Lambda_{film}}} \sigma \pi r_{contact}^2 \left(T_{film}^4 - T_0^4\right) \tag{S13}$$

$$\Lambda_{film} = -\frac{d_{film}}{ln\left[\left(\frac{\lambda_{film}}{\sigma \cdot d_{film}}\right) \cdot \frac{(T_{film} - T_0)}{\left(T_{film}^4 - T_0^4\right)}\right]} \tag{S14}$$

References

S1 DETHERM. 2015. http://www.dechema.de/Detherm.html. Accessed February 9, 2016.

S2 A. Altes, R. Heiderhoff and L. J. Balk, *Journal of Physics D: Applied Physics*, 2004, **37**, 952–963.

S3 A.-K. Geinzer, University of Wuppertal, 2010.

S4 G. B. M. Fiege, A. Altes, R. Heiderhoff and L. J. Balk, *Journal of Physics D: …*, 1999, **13**, L13–L17.

S5 W. E.M., *Physics education (U.K.)*, 1975, **10**, 25–27.

S6 M. Carla, *American Journal of Physics*, 2013, **81**, 512–517.

S7 A. Majumdar, *Journal of Heat Transfer*, 1993, **115**, 7–16.

S8 E. T. Swartz and R. O. Pohl, *Reviews of Modern Physics*, 1989, **61**, 606–668.

S9 C. S. Gorham, J. T. Gaskins, G. N. Parsons, M. D. Losego and P. E. Hopkins, *Applied Physics Letters*, 2014, **104**, 253107.

S10 N. Oka, R. Arisawa, A. Miyamura, Y. Sato, T. Yagi, N. Taketoshi, T. Baba and Y. Shigesato, *Thin Solid Films*, 2010, **518**, 3119–3121.

S11 D. J. Kim, D. S. Kim, S. Cho, S. W. Kim, S. H. Lee and J. C. Kim, *International Journal of Thermophysics*, 2004, **25**, 281–289.

S12 A. A. Wilson, M. Muñoz Rojo, B. Abad, J. A. Perez, J. Maiz, J. Schomacker, M. Martín-Gonzalez, D.-A. Borca-Tasciuc and T. Borca-Tasciuc, *Nanoscale*, 2015, 7, 15404–15412.